Journal of Solid State Chemistry 184 (2011) 1875–1881

Contents lists available at ScienceDirect

Journal of Solid State Chemistry

journal homepage: www.elsevier.com/locate/jssc

Flux growth of a new cobalt–zinc–tin ternary phase $Co_{7+x}Zn_{3-x}Sn_8$ and its relationship to CoSn

Patricia C. Reynolds, Milorad Stojanovic [1], Susan E. Latturner *

Department of Chemistry and Biochemistry, Florida State University, Tallahassee, FL 32306, United States

ARTICLE INFO

Article history:
Received 22 February 2011
Received in revised form
10 May 2011
Accepted 15 May 2011
Available online 26 May 2011

Keywords:
Metal flux growth
Tin flux
Supercell
Eutectic
Crystallography
Solder

ABSTRACT

The intermetallic compound $Co_{7+x}Zn_{3-x}Sn_8$ ($-0.2 < x < 0.2$) forms from the reaction of cobalt in zinc/tin eutectic flux. This phase has a new structure type in orthorhombic space group *Cmcm*, with unit cell parameters $a=4.138(1)$ Å, $b=12.593(4)$ Å, and $c=11.639(4)$ Å ($Z=2$; $R_1=0.0301$). Varying the amount of cobalt in the synthesis leads to formation of a superstructure in space group *Pnma*, with lattice parameters $a=12.5908(2)$ Å, $b=11.6298(3)$ Å, and $c=8.2704(2)$ Å ($Z=4$; $R_1=0.0347$). A Co/Zn mixed site and a partially occupied Co site in the *Cmcm* structure order to form the *Pnma* supercell. TGA/DSC studies indicate that the binary phase CoSn initially forms in the flux at 1173 K, and then reacts with the zinc in the cooling solution to form the ternary structure at 823 K. This phase exhibits Pauli paramagnetic behavior.

1. Introduction

Metal fluxes are useful media for exploratory synthesis of intermetallics and Zintl phases and for growth of large single crystals for physical property measurements [1]. Metals commonly used as solvents in flux synthesis are inexpensive and low melting. Tin has been widely used as a flux; reactions in molten tin have led to recent discovery of new phases such as $RESn_{1+x}Ge_{1-x}$ and OsB [2,3]. Tin melts have also enabled the growth of large crystals of known phases, including the $Ba_{1-x}K_xFe_2As_2$ superconductors, which have been of particular interest recently [4,5]. We have been investigating lowering the melting point of tin by combining it with other metals to form eutectic fluxes. The Zn/Sn phase diagram is a simple eutectic system with no binary phases, featuring a eutectic at 15% Zn with a melting point of 473 K [6]. This eutectic is sold commercially for use as a lead-free solder (for example, it is marketed by Indium Corporation as Indalloy 201, recommended for soldering to high aluminum alloys). Interactions of metals with this Zn/Sn melt is therefore of interest to researchers in a number of fields, particularly given the worldwide interest in finding alternatives to lead-based solders [7,8].

In this study, cobalt was reacted in Zn/Sn eutectic to explore the growth of potentially magnetic materials. Complex peritectic behavior is seen during this reaction, similar to that observed for cobalt in pure tin flux (cobalt reacts in tin to form CoSn at high temperatures, which further reacts with the flux as the temperature is lowered, forming $CoSn_2$ and $CoSn_3$) [9]. In Zn/Sn flux, the binary CoSn forms at 1173 K, and then reacts at lower temperatures to form a new ternary phase $Co_{7+x}Zn_{3-x}Sn_8$ ($-0.2 < x < 0.2$). Variation in reactant ratio leads to two different structures for the ternary phase, a subcell which crystallizes in the *Cmcm* space group and a supercell, which crystallizes in the *Pnma* space group. These two compounds are also structurally related to the CoSn binary phase.

2. Material and Methods

2.1. Synthesis

Co powder (Alfa-Aesar, 99.8%), Zn powder (Alfa-Aesar, 99.8%), and Sn granules (Alfa-Aesar, 99.9%) were combined in a 2:1.5:8.5 millimolar ratio in an alumina crucible. A second crucible containing silica wool was placed upside down above the reaction crucible to act as a filter during centrifugation. This setup was then placed in a fused silica tube, sealed under vacuum at 10^{-2} Torr, and then heated to 1173 K in 6 h, held at 1173 K for 24 h, cooled to 973 K over 36 h, held there for 24 h, and then cooled to 593 K over 36 h. At 593 K, the sample was inverted and centrifuged to remove the excess molten Zn/Sn flux. The crystals removed from the alumina crucible had a square shaped appearance and were silver colored and reflective.

In order to explore the phase width of this compound, reactions were carried out with different amounts of Co in the Zn/Sn eutectic. Co/Zn/Sn reactions were prepared with millimolar

* Corresponding author. Fax: +850 644 8281.
E-mail address: latturne@chem.fsu.edu (S.E. Latturner).
[1] Present address: Department of Chemistry, University of South Alabama, Mobile, AL 36688, United States.

0022-4596/$ - see front matter © 2011 Elsevier Inc. All rights reserved.
doi:10.1016/j.jssc.2011.05.019

ratios y:1.5:8.5, with y varying in increments of 0.5 from 1.0 up to 3.0 mmoles. These reactions were carried out in alumina crucibles as described above. Products of reactions with 1.0 or 3.0 millimoles of Co had a flatter, more plate-like appearance, noticeably different from the more blocky appearance of products of reactions with 2 millimoles of Co.

After the structure of the ternary phase was determined, stoichiometric synthesis was attempted using 3.5 millimoles of Co, 1.5 millimoles of Zn, and 4 millimoles of Sn. These reactants were loaded into an alumina crucible, which was placed in a fused silica tube and sealed under vacuum at 10^{-2} Torr. The ampoule was then heated from 298 to 1173 K in 2 h, held at 1173 K for 6 h, cooled to 300 K in 6 h and removed from the oven.

2.2. Elemental analysis

Elemental analysis was performed on all samples using a JEOL 5900 scanning electron microscope with energy-dispersive X-ray spectroscopy (EDXS) capabilities. Flux-grown crystals from each reaction were affixed to an aluminum SEM puck using carbon tape, and positioned so that flat faces were perpendicular to the electron beam. Samples were analyzed using 30 kV accelerating voltage and an accumulation time of 60 s.

Table 1
Crystallographic parameters for the $Co_{7+x}Zn_{3-x}Sn_8$ subcell and supercell structures.

	$Co_{7.2(1)}Zn_{2.9(1)}Sn_8$ (subcell)	$Co_{6.8(4)}Zn_3Sn_8$ (supercell)
Reactant ratio (Co/Zn/Sn)	2:1.5:8.5	1:1.5:8.5
Formula weight (g/mol)	1556.96	1558.04
Crystal system	orthorhombic	orthorhombic
Space group	*Cmcm*	*Pnma*
a (Å)	4.139(1)	12.5908(2)
b (Å)	12.593(4)	11.6298(3)
c (Å)	11.640(4)	8.2704(2)
Z	2	4
Volume	606.7(3)	1211.02(5)
Density, calc (g/cm^3)	8.585	8.485
Temperature (K)	293	
Radiation	Mo$K\alpha$	
Index ranges	$-5 \le h \le 5$ $-16 \le k \le 16$ $-15 \le l \le 15$	$-20 \le h \le 20$ $-18 \le k \le 15$ $-11 \le l \le 13$
Reflections collected	3318	12,538
Unique data/parameters	430/41	2618/99
μ (mm^{-1})	31.33	30.97
R_1/wR_2[a]	0.0301/0.0728	0.0347/0.0869
R_1/wR_2 (all data)	0.0314/0.0739	0.0580/0.0968
Residual peak/hole (e$^-$Å^{-3})	1.37/−1.72	2.70/−2.75

[a] $R_1 = \Sigma \| F_o | - | F_c \| / \Sigma | F_o |$; $wR_2 = [\Sigma[w(F_o^2 - F_c^2)^2] / \Sigma[w(F_o^2)^2]]^{1/2}$.

2.3. X-ray diffraction

For each single crystal experiment, a small single crystal was selected and mounted on a glass fiber using epoxy. Single crystal X-ray diffraction data were collected at room temperature using a Bruker AXS APEX2 CCD diffractometer with a Mo radiation source. Processing of the data was accomplished using the program SAINT. An absorption correction was applied to the data using the SADABS program [10]. Refinement of the structure was performed using the SHELXTL package [11]. X-ray diffraction data were collected for representative crystals from reactions with 1 and 2 millimolar amounts of Co reactant. The crystallographic data collection parameters are summarized in Table 1; atomic positions and bond lengths are listed in Tables 2–4. Further details of the crystal structure investigation may be obtained from Fachinformationszentrum Karlsruhe, 76344 Eggenstein-Leopoldshafen, Germany (fax: (+49)7247 808 666; e-mail: crysdata@fiz-karlsruhe.dea, http://www.fiz-karlsruhe.de/request_for_deposited_data.html) on quoting the CSD numbers CSD-422703 (subcell) and CSD-422704 (supercell).

Powder X-ray diffraction was used to explore the possible phase width associated with this compound. Samples of the solid product from each flux synthesis were ground with a small amount of silicon to act as an internal standard to allow accurate determination of unit cell parameters. Powder X-ray diffraction data were collected using an original diffraction setup based on a Huber imaging plate Guinier camera 670 that uses Cu$K\alpha_1$ radiation ($\lambda = 1.54060$ Å) with a Ge crystal monochromator. The accompanying JADE software was used to analyze the powder patterns. The theoretical powder pattern calculated from the crystal structure was compared to the data for products of reactions at different millimolar ratios (see Supplementary Content, Fig. S1). Refinement for each sample indicated very little change in unit cell parameters. Powder XRD data were also collected on samples of the product of attempted stoichiometric synthesis, and on flux-grown $Co_{7+x}Zn_{3-x}Sn_8$ samples after thermal analysis (to identify decomposition products); see Supplementary Content, Fig. S2.

2.4. Magnetic susceptibility

Magnetic measurements were carried out with a Quantum Design MPMS SQUID magnetometer at temperatures between 2 and 300 K. Crystals were ground into a fine powder and put into a capsule with the cap inverted to insure that the powder was tightly pressed and immobile. The capsule was placed in a plastic straw and placed into the magnetometer. Temperature dependent susceptibility data from 2 to 300 K were collected at applied fields of 500–1000 G, and field dependence data was collected at 3 K. A superconducting transition was observed at 3.7 K at low applied fields. This indicated a Sn impurity (likely from residual traces of flux) which was corrected for by increasing the applied field to 1000 G, above the critical field for Sn.

Table 2
Atom positions for the *Cmcm* subcell structure of $Co_{7.2(1)}Zn_{2.9(1)}Sn_8$.

Atom	Wyckoff site	Occupancy	*x*	*y*	*z*	U_{eq}[a]
Sn(1)	8*g*	0.505(2)	0.4373(2)	0.48324(8)	¼	0.0076(3)
Sn(2)	8*f*		0	0.34253(4)	0.02024(5)	0.0114(2)
Sn(3)	4*c*		0	0.70920(6)	0.25	0.0112(2)
Co(1)	8*f*		0	0.16053(8)	0.12905(8)	0.0110(3)
Co(2)	8*f*	0.535(4)	0	0.5204(1)	0.1357(4)	0.0059(4)
Zn(3)/Co(3)	4*c*	0.45(5)/0.55(5)	0	0.3430(1)	0.25	0.0082(5)
Zn(1)	4*a*		0	0	0	0.0092(3)

[a] U_{eq} is defined as 1/3 of the trace of the orthogonalized U_{ij} tensor.

Table 3
Atom positions for the *Pnma* supercell structure of $Co_{6.8(4)}Zn_3Sn_8$.

Atom	Wyckoff site	Occupancy	*x*	*y*	*z*	U_{eq}[a]
Co(1)	8*d*		0.08433(6)	0.13056(8)	0.3726(1)	0.0078(1)
Co(2)	8*d*		0.22929(6)	0.13573(8)	0.1261(1)	0.0081(1)
Co(3)	8*d*	0.904(4)	0.40499(7)	0.62746(9)	0.3789(1)	0.0078(2)
Co(4)	4*c*		0.41104(8)	0.25	0.6253(1)	0.0066(2)
Zn(1)	8*d*		0.24824(5)	0.00154(7)	0.3758(1)	0.0098(1)
Zn(2)	4*c*		0.40301(8)	0.25	0.1251(1)	0.0114(2)
Sn(1)	8*d*		0.08981(2)	0.52845(4)	0.12653(7)	0.0088(1)
Sn(2)	8*d*		0.40468(3)	0.01162(4)	0.12422(7)	0.0086(1)
Sn(3)	4*c*	0.88(5)	0.0376(3)	0.25	0.120(1)	0.0089(5)
Sn(3a)	4*c*	0.12	0.044(1)	0.25	0.092(4)	0.0089
Sn(4)	4*c*		0.04324(5)	0.25	0.63317(1)	0.0102(1)
Sn(5)	4*c*	0.968(3)	0.26484(5)	0.25	0.4068(1)	0.0084(1)
Sn(5a)	4*c*	0.032	0.260(1)	0.25	0.340(4)	0.0084
Sn(6)	4*c*		0.26867(5)	0.25	0.84411(7)	0.0097(1)

[a] U_{eq} is defined as 1/3 of the trace of the orthogonalized U_{ij} tensor.

Table 4
Comparison between selected bond lengths in the subcell and supercell structures of $Co_{7+x}Zn_{3-x}Sn_8$.

***Cmcm* subcell**		***Pnma* supercell**	
Bonds	Length (Å)	Equivalent bonds	Length (Å)
Zn(1)–Co(1)	2.519(1) × 2	Zn(1)–Co(1), Zn(1)–Co(3)	2.552(1), 2.479(1)
Zn(1)–Co(2)	2.616(1) × 4	Zn(1)–Co(2)	2.600(2), 2.630(2)
Zn(1)–Sn(2)	2.8758(7) × 4	Zn(1)–Sn(2), Zn(1)–Sn(1)	2.820(1), 2.868(1), 2.890(1)
Co(3)/Zn(3)–Sn(1)	2.528(1) × 2	Zn(2)–Sn(5)	2.53(2)
		Co(4)–Sn(3)	2.547(2)
Co(3)/Zn(3)–Co(2)	2.601(2) × 2	Zn(2)–Co(2)	2.559(1)
Co(3)/Zn(3)–Sn(3)	2.669(1) × 2	Zn(2)–Sn(3), Zn(2)–Sn(4);	2.701(8), 2.771(2);
		Co(4)–Sn(3), Co(4)–Sn(4)	2.586(8), 2.600(2)
Co(3)/Zn(3)–Sn(2)	2.674(1) × 2	Zn(2)–Sn(2)	2.7724(5)
		Co(4)–Sn(1)	2.5766(5)
Co(3)/Zn(3)–Co(1)	2.695(1) × 2	Zn(2)–Co(1)	2.672(1)
		Co(4)–Co(3)	2.720(1)

2.5. Thermal analysis

TGA/DSC analysis was performed using a TA Instruments Q600 to investigate the stability of the products and to study their formation in the flux. Data were collected on $Co_{7+x}Zn_{3-x}Sn_8$ samples synthesized from a 2:1.5:8.5 mmol Co/Zn/Sn reaction; individual crystals of the compound were selected and ground into powder. This powder was loaded into a small alumina cup placed in the instrument; argon gas was flowed at a rate of 100 mL/min in order to prevent oxidation of the sample during heating. Each sample was heated at 10°/min to 1273 K and cooled from 1273 to 298 K at 5°/min. Powder X-ray diffraction data was taken afterwards to determine the thermal decomposition products. A DSC in-situ study of the flux reaction was carried out by preparing a scaled-down version of the 2:1.5:8.5 mmol mixture, with the total quantity of reactants reduced to a net mass of 150 mg to fit into the alumina sample cup. This miniature flux reaction was heated at 10°/min to 1273 K and cooled from 1273 to 298 K at 5°/min under a flow of argon gas.

3. Results and discussion

3.1. Reactions of cobalt in Zn/Sn flux

Our exploration of the reaction of cobalt in Zn/Sn eutectic flux was motivated by the fact that different phases were isolated from identical reaction compositions if they were centrifuged or quenched at different temperatures. This phenomenon is seen in the Co/Sn binary system; reaction of cobalt in an excess of tin yields CoSn, $CoSn_2$, and $CoSn_3$ which crystallize at different temperatures [9]. Similar behavior is also seen in more complex flux reactions. For instance, two structurally related layered phases Ce_2PdGa_{12} and $CePdGa_6$ can be crystallized from identical gallium flux reactions centrifuged at different temperatures [12]. Likewise, $LaFe_{13-x}Al_x$ and $La_6Fe_{13-x}Al_{1+x}$ (comprised of similar building blocks) can be isolated at different temperatures from reactions of aluminum in La/Fe eutectic flux [13].

A 2:1.5:8.5 Co/Zn/Sn reaction yields CoSn if centrifuged above 873 K; if it is instead allowed to cool to 593 K and centrifuged, the new ternary phase $Co_{7+x}Zn_{3-x}Sn_8$ is isolated. This behavior is apparent when a smaller scale flux reaction is monitored using DSC/TGA (see Fig. 1). At high temperature, cobalt reacts in the flux leading to crystallization of the binary phase CoSn, indicated by an exotherm at 1173 K during cooling. This compound reacts with the Zn/Sn solution to form $Co_{7+x}Zn_{3-x}Sn_8$ when cooled to 823 K (inset of Fig. 1). Changing the amount of cobalt does not affect the temperature of the formation of the ternary phase. If the reaction is centrifuged at or near this temperature, the transition of one phase to another can be captured in progress; the resultant product features hexagonal rod-shaped crystals of the binary phase CoSn with protrusions of the ternary phase $Co_{7+x}Zn_{3-x}Sn_8$ growing on them (SEM image shown in Fig. 2). If the flux reaction is instead allowed to cool further, the ternary phase becomes predominant, with much smaller amounts of CoSn as a byproduct (see Supplementary Content, Fig. S1). An exotherm at 473 K indicates freezing of the eutectic flux.

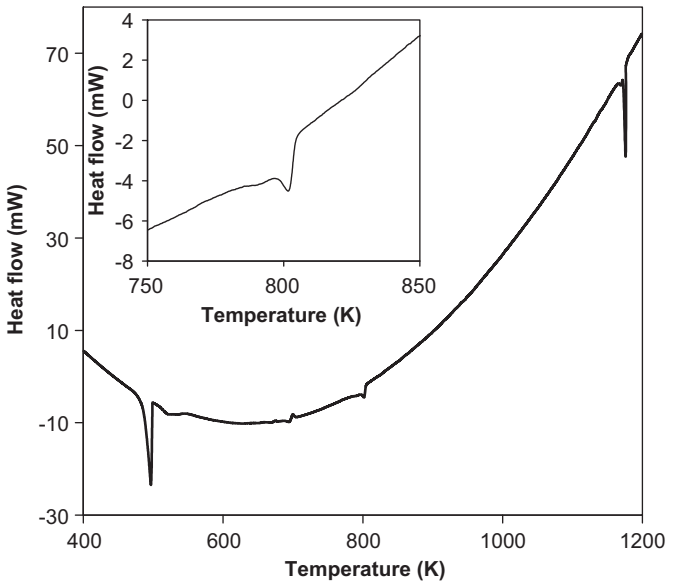

Fig. 1. Differential scanning calorimetry data for the reaction of cobalt in Zn/Sn eutectic, taken as the flux reaction was cooled from 1273 K to room temperature. The inset highlights the transition from CoSn to $Co_{7+x}Zn_{3-x}Sn_8$.

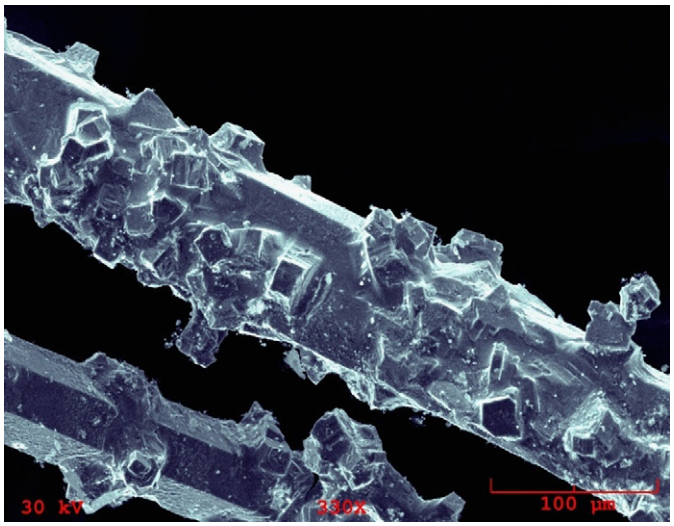

Fig. 2. SEM image taken of the product isolated from the reaction of cobalt in Zn/Sn eutectic when centrifuged at 823 K. Protrusions on the rods are the ternary phase (elemental analysis indicates presence of Co, Zn, and Sn); the hexagonal rods themselves contain only Co and Sn.

Flux reactions cooled to 593 K and centrifuged to remove the excess flux yield well-formed crystals of $Co_{7+x}Zn_{3-x}Sn_8$, up to 2 mm on a side. The yield based on Co is approximately 80%, with small amounts of CoSn as a byproduct. The phase width of the title compound is very small ($-0.2 < x < 0.2$); variations in reaction ratios did not cause significant changes in the stoichiometry of the product (as determined by elemental analysis and powder and single crystal XRD data). This phase is stable to air; no visual oxidation or degradation of the material is observed for samples exposed to atmospheric oxygen over the course of several months. It is not sensitive to water or 1 M HCl. When heated under a flow of argon during TGA/DSC analysis, there was a loss of 8.4% mass above 823 K, which was attributed to the loss of Zn and sublimes readily [14]. This loss of mass occurs at the same temperature of the transition from the binary to the ternary phase. The resulting sample was analyzed by powder X-ray diffraction. Small amounts of $Co_{7+x}Zn_{3-x}Sn_8$ were still present, but additional peaks corresponding to binary phases CoSn and $CoSn_2$ predominated (see Supplementary Content, Fig. S2).

$Co_{7+x}Zn_{3-x}Sn_8$ can also be synthesized from a stoichiometric reaction of the elements, although not in pure form (contaminants include tin and CoSn; see Supplementary Content, Fig. S2). Powder XRD patterns were calculated based on the subcell and supercell crystal structures of $Co_{7+x}Zn_{3-x}Sn_8$ (*vide infra*); these were compared to the observed powder pattern of the stoichiometric product. There are very subtle differences between the calculated powder patterns of the subcell structure (in space group *Cmcm*) and the supercell structure (one axis doubled, in space group *Pnma*). Additional peaks in the *Pnma* structure appear at low 2θ and are also found between 10° and 25° 2θ, 34° and 44° 2θ, and 46° and 56° 2θ. The powder pattern of the product of stoichiometric synthesis seems to indicate formation of the supercell, although the presence of diffraction peaks due to contaminants makes this unclear.

3.2. $Co_{7+x}Zn_{3-x}Sn_8$ subcell and supercell crystal structures

$Co_{7+x}Zn_{3-x}Sn_8$ forms in two related structures, depending on the initial Co concentration of the flux reaction. Single crystal data were taken for samples from several different Co/Zn/Sn reactions with ratios *y*:1.5:8.5 mmol. When 2 mmol Co were used, a subcell structure forms in the orthorhombic space group *Cmcm* (Fig. 3a). On the other hand, products of reactions containing 1 or 3 mmol Co have a supercell structure in orthorhombic space group *Pnma* (Fig. 3b). The axes of the unit cells are related as follows: $a_{super} = b_{sub}$; $b_{super} = c_{sub}$; $c_{super} = 2a_{sub}$. While the amount of cobalt reactant in the flux does appear to reproducibly determine whether the structure forms in the subcell or supercell, it should be noted that the stoichiometry of the product does not change. Both the subcell and supercell structures have very similar elemental ratios (within estimated standard deviations; see Table 1).

To simplify consideration of the highly complex $Co_{7+x}Zn_{3-x}Sn_8$ structure, Fig. 3c and d depict the *Cmcm* and *Pnma* structures with the tin atoms removed, and highlight the doubled unit cell axis going from the subcell to the supercell. The change in symmetry and cell size appears to stem from the ordering of cobalt and zinc on individual 4*c* sites in the supercell (atoms Zn(2) and Co(4) in Table 3). These sites correspond to a single 4*c* site in the subcell, which refines as occupied by 45(5)%/55% (atom Zn(3)/Co(3) in Table 2 and Fig. 3c). Additional differences are found in other cobalt sites, which form a zig–zag chain running parallel to one axis in the structure (along the *a*-axis in the subcell; along the *c*-axis in the supercell). In the subcell, this chain is comprised of Co(1) and Co(2) atoms (both in 8*f* sites). The Co(2) site is half-occupied. It is adjacent to a tin site (Sn(1)), which has a symmetry equivalent 0.56 Å away which mandates half-occupancy for this tin atom. One of these symmetry equivalents is a very short distance (2.2 Å) from the Co(2) site, which requires half occupancy for the cobalt atom. In the supercell, a similar situation occurs with tin atoms occupying split sites leading to short Co–Sn distances. However, this causes ordered vacancies in the cobalt zig–zag chain in the supercell, instead of the random partial occupancy seen in the subcell.

3.3. Structural relationship to CoSn

The $Co_{7+x}Zn_{3-x}Sn_8$ structure features predominantly heteroatomic bonding; there are no Zn–Zn or Sn–Sn bonds, and while there are Co–Co bonds, cobalt exhibits far shorter bonds to neighboring Zn and Sn (see Table 4). It is difficult to break the

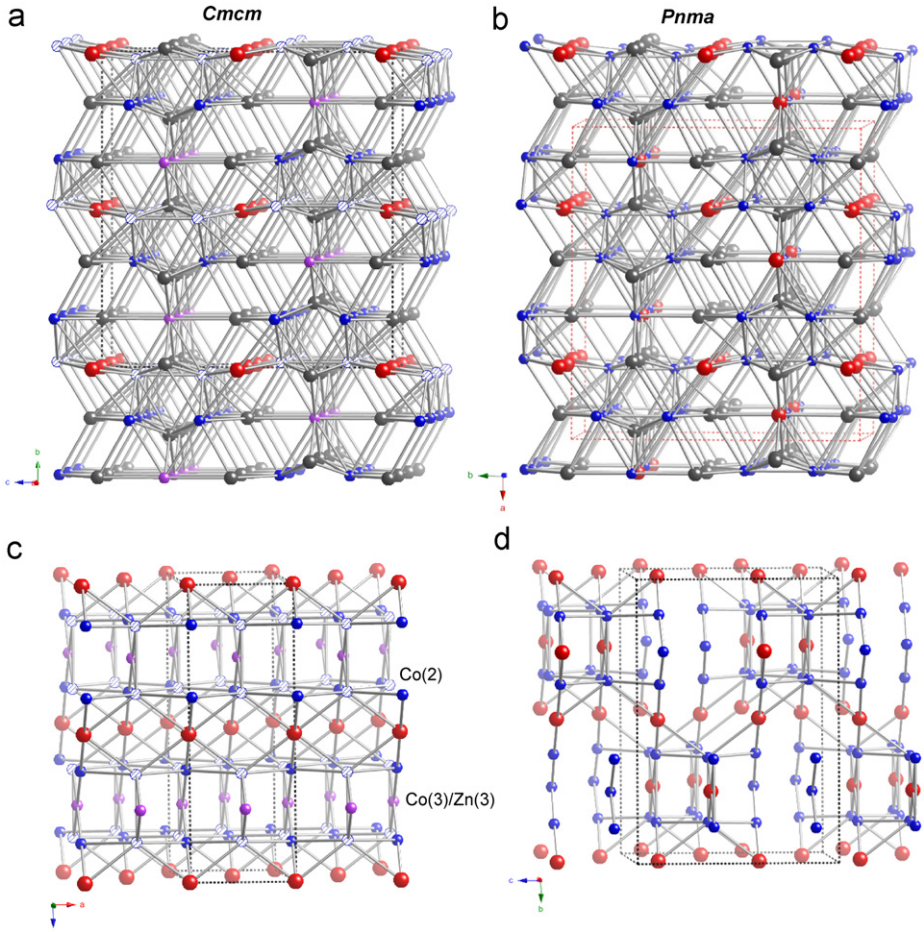

Fig. 3. Structure of $Co_{7+x}Zn_{3-x}Sn_8$. Unit cells are indicated by dashed lines. Cobalt atoms are represented by blue spheres, zinc atoms by red spheres, and tin atoms by gray spheres; mixed Co/Zn sites are represented by purple spheres, and half-occupied cobalt sites by blue hatched spheres. (a) *Cmcm* subcell structure, viewed down the *a*-axis. (b) *Pnma* supercell structure, viewed down the *c*-axis. (c) *Cmcm* subcell structure with tin atoms removed, viewed down the *b*-axis. (d) *Pnma* supercell structure with tin atoms removed, viewed down the *a*-axis. (For interpretation of the references to color in this figure legend, the reader is referred to the web version of this article.)

overall structure down into coordination polyhedra as is often done for more polar intermetallics containing highly electropositive metals such as alkaline earths or lanthanide elements, which often exhibit highly symmetric bonding environments that can be viewed as distinct building blocks. While such easily notable coordination spheres are not present in the title compound, some structural moieties are found which are similar to those in the CoSn binary phase. In particular, the cluster of Sn and Co atoms surrounding the Co/Zn mixed site (site 4*c* in the subcell) is also found in CoSn; this is shown in Fig. 4. The Co–Sn and Co–Co bond lengths in this moiety and throughout the structure are similar to those in CoSn, which features Co–Co bonds of 2.639 Å and Co–Sn bonds of 2.619 and 2.639 Å [15]. Comparable bond lengths are also found in ternary phases such as $Mg_2Co_3Sn_{10}$; Co–Sn bonds in this compound range from 2.604 to 2.772 Å [16].

The presence of these similar structural building blocks in $Co_{7+x}Zn_{3-x}Sn_8$ and CoSn may enable CoSn to act as a template for the formation of the ternary phase. The conversion of the binary phase to the ternary phase may be attributed to the presence of Zn in the solution. As the binary phase begins to precipitate out of the flux, the remaining solvent mixture becomes richer in zinc. As the reaction temperature is lowered the zinc begins to migrate into the CoSn structure, substituting for Co and leading to formation of the ternary phase from the feedstock of CoSn. Reactions that were carried out below the formation temperature of CoSn produced this phase as well; however, the yield was much lower and $CoSn_3$ was found as a competing phase.

3.4. Magnetic characterization

Cationic cobalt in coordination complexes and ionic compounds exhibits a magnetic moment associated with its oxidation state and the local ligand field environment. The magnetism of cobalt in intermetallics is more complex due to the formation of bands by the interacting *d*-orbitals. The magnetic moment associated with cobalt will depend on the filling of these bands and their vicinity to the Fermi level. In general, cobalt atoms in cobalt-poor intermetallics do not possess magnetic moments. Phases such as $Mg_2Co_3Sn_{10+x}$ and $La_3Co_4Sn_{13}$ exhibit only Pauli paramagnetism due to conduction electrons [16,17]. Cobalt-rich intermetallics do feature cobalt moments; the hard magnetic properties of $SmCo_5$ are due to the ordering of magnetic moments on Co (1.4–1.5 μ_B per Co) [18]. Magnetic moments ranging from 0.3 to 1.9 μ_B per Co are observed for phases such as $Co_3Sn_2S_2$, $R_6Co_{13}Sn$, and $RCo_{12}B_6$ (R=rare earth) [18,19].

The behavior of $Co_{7+x}Zn_{3-x}Sn_8$ is of interest since it forms in two slightly different structure types and its stoichiometry is in the intermediate regime between "cobalt-rich" and "cobalt-poor" intermetallics. Magnetic susceptibility data were collected on samples crystallizing in *Cmcm* or *Pnma* structures; the data are shown in Fig. 5. Both datasets appear to be dominated by Pauli paramagnetism, with Curie tails at low temperature possibly due to traces of cobalt oxides formed on particle surfaces. A modified Curie–Weiss law was used to fit the data ($\chi=(C/T-\theta)+\chi_0$, where C and θ are the Curie and Weiss constants corresponding to the

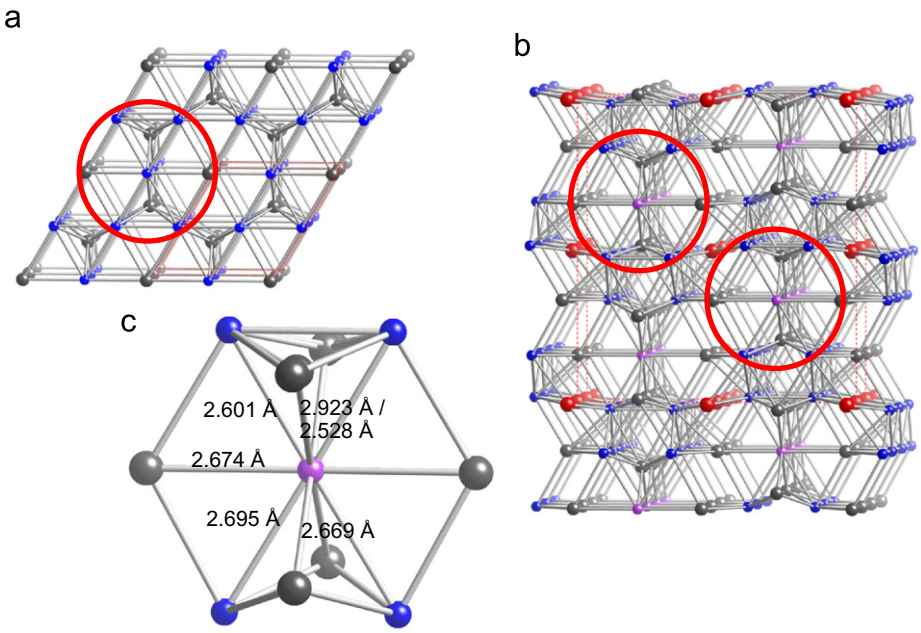

Fig. 4. Comparison between the structures of CoSn and $Co_{7+x}Zn_{3-x}Sn_8$. (a) The hexagonal CoSn structure viewed down the *c*-axis; cobalt atoms indicated by blue spheres. (b) The *Cmcm* subcell structure of $Co_{7+x}Zn_{3-x}Sn_8$, viewed down the *a*-axis. (c) The common building block of the cobalt site (or Co/Zn site in the ternary phase) and its coordination environment.

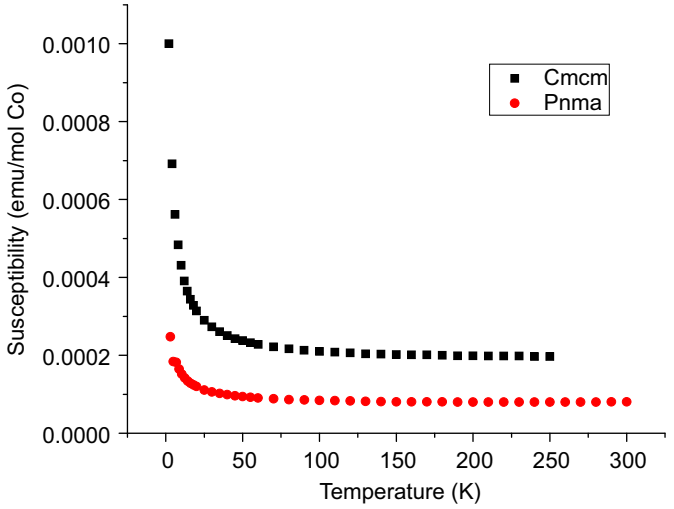

Fig. 5. Inverse magnetic susceptibility data for the $Co_{7+x}Zn_{3-x}Sn_8$ phase in both subcell and supercell structures.

cobalt moments, and χ_0 is the temperature independent Pauli paramagnetism). The cobalt moments derived from the Curie constants were negligible for both samples (0.003 and 0.001 μ_B per cobalt atom for the subcell and supercell structured samples, respectively), as were the Weiss constants (below 3.0 K in both cases). The Pauli paramagnetism values of 0.00018(4) emu/mol for the subcell structured sample and 0.00010(8) emu/mol for the supercell structured sample are in the 10^{-3}–10^{-4} emu/mol range expected for intermetallics.

4. Conclusions

A new ternary phase was found in the Co/Zn/Sn system, growing as well-formed crystals from a Zn/Sn eutectic flux. Quenching reactions at different temperatures played an integral role in discovery of this compound, since it forms as a low temperature phase from the reaction of CoSn with the Zn/Sn melt. This emphasizes the importance of exploring the effects of temperature in metal flux reactions. The reason is not clear as to why the cobalt reactant concentration in the flux determines the formation of $Co_{7+x}Zn_{3-x}Sn_8$ in the subcell or supercell structure. Our initial investigations into reactions of other metals (iron and nickel) in Zn/Sn flux indicate that they form similar compounds, both crystallizing in the *Cmcm* subcell structure. Compared to the cobalt analog, the $Fe_{7+x}Zn_{3-x}Sn_8$ phase has slightly larger unit cell parameters (a=4.140(1) Å, b=12.605(3) Å, c=11.621(3) Å) and $Ni_{7+x}Zn_{3-x}Sn_8$ exhibits slightly smaller cell parameters (a=4.1171(5) Å, b=12.582(1) Å, c=11.616(1) Å), as expected from their relative atomic radii. The formation of these intermetallics in Zn/Sn eutectic flux reactions may have important implications on the use of Zn/Sn solder with transition metal alloys.

Acknowledgments

This research made use of the Scanning Electron Microscope facilities of the Physics Department at Florida State University. Financial support from the NSF (Grant DMR-05-47791) is gratefully acknowledged.

Appendix A. Supporting information

Supplementary data associated with this article can be found in the online version at doi:10.1016/j.jssc.2011.05.019.

References

[1] M.G. Kanatzidis, R. Pottgen, W. Jeitschko., Angew. Chem. Int. Ed. 44 (2005) 6996–7023.
[2] P.H. Tobash, J.J. Meyers, G. DiFilippo, S. Bobev, F. Ronning, J.D. Thompson, J.L. Sarrao., Chem. Mater. 20 (2008) 2151–2159.
[3] B.P.T. Fokwa, P.R.N. Misse, M. Gilleβen, R. Dronskowski, J. Alloys Cmpds. 489 (2010) 339–342.
[4] N. Ni, S.L. Bud'ko, A. Kreyssig, S. Nandi, G.E. Rustan, A.I. Goldman, S. Gupta, J.D. Corbett, A. Kracher, P.C. Canfield, Phys. Rev. B 78 (2008) 014507.

[5] J.L. Mathieu, S.E. Latturner, Chem. Commun. (2009) 4965–4967.
[6] T.B. Massalski, H. Okamoto., Binary Alloy Phase Diagrams, 2nd ed., ASM International, Materials Park, OH, 1990.
[7] V.I. Dybkov, V.G. Khoruzha, V.R. Sidorko, K.A. Meleshevich, A.V. Samelyuk, D.C. Berry, K. Barmak, J. Mater. Sci. 44 (2009) 5960–5979.
[8] F. Gao, F. Cheng, H. Nishikawa, T. Takemoto, Mater. Lett. 62 (2008) 2257–2259.
[9] A. Lang, W. Jeitschko, Z. Metallkd 87 (1996) 759–764.
[10] SAINT, version 6.02a; Bruker AXS, Inc.: Madison, WI, 2000.
[11] G.M. Sheldrick, SHELXTL NT/2000, version 6.1, Bruker AXS, Inc., Madison, WI, 2000.
[12] R.T. Macaluso, J.N. Millican, S. Nakatsuji, H.O. Lee, B. Carter, N.O. Moreno, Z. Fisk, J.Y. Chan., J. Solid State Chem. 178 (2005) 3547–3553.
[13] E.M. Benbow, N.S. Dalal, S.E. Latturner, J. Solid State Chem. 182 (2009) 3055–3062.
[14] A.N. Nesmeyanov., Vapor Pressure of the Chemical Elements, Elsevier, Amsterdam, 1963.
[15] P. Villars, L.D. Calvert, Pearson's Handbook—Crystallographic Data for Intermetallic Phases, Materials Park, OH, ASM International, 1998.
[16] M. Schreyer, G. Kraus, T.F. Fassler, Z. Anorg. Allg. Chem. 630 (2004) 2520–2526.
[17] G. Zhong, X. Lei, J. Mao, Phys. Rev. B 79 (2009) 094424.
[18] P. Vaqueiro, G.G. Sobany, Solid State Sci. 11 (2009) 513–518.
[19] A. Szytula, J. Leciejewicz, Handbook of Crystal Structures and Magnetic Properties of Rare earth Intermetallics, CRC Press, Boca Raton, FL, 1994.